BiOBr-rice husk carbon composite for antibiotic degradation

Bosely Anne Bose, Ange Nzihou, Daniel Thangadurai, Abhijit Saha, Nandakumar Kalarikkal

BiOBr-rice husk carbon composite for antibiotic degradation

Bosely Anne Bose [a], Ange Nzihou [b,c], Daniel Thangadurai [d], Abhijit Saha [e,f], Nandakumar Kalarikkal [a,f,g],

[a] School of Pure and Applied Physics, Mahatma Gandhi University, Kottayam-686 560, Kerala, India
[b] Universite de Toulouse, IMT Mines Albi, RAPSODEE CNRS UMR 5302, Campus Jarlard, F.81013, Albi, Cedex 09, France
[c] Andlinger Center for Energy and the Environment, Princeton University, Princeton, NJ, NJ, 08544, USA
[d] Department of Chemistry, Centre for Research and Development, KPR Institute of Engineering and Technology, Coimbatore, 641407, Tamil Nadu, India
[e] UGC-DAE Consortium for Scientific Research, Kolkata Centre, III/LB-8 Bidhannagar, Kolkata, 700106, West Bengal, India
[f] International and Inter University Centre for Nanoscience and Nanotechnology, Mahatma Gandhi University, Kottayam, 686 560, Kerala, India
[g] University Centre for Ultrafast Studies, Mahatma Gandhi University, Kottayam, 686 560, Kerala, India

A B S T R A C T

Highly efficient visible light photocatalysts are necessary to address the water pollution caused by antibiotics. In the present study, bismuth oxybromide-rice husk-derived carbon (BiOBr-RHC) composites (with different wt% of RHC) were prepared via a simple solid-state method. Results of the studies indicate that the use of rice husk carbon has a considerable effect on the degradation of the commonly used fluoroquinolone antibiotic norfloxacin (NOR). BiOBr-RHC-10 exhibits the highest catalytic degradation towards NOR under visible light irradiation among the developed composite catalysts. Introducing carbon in the composites provides better separation of charge carriers, thereby reducing the recombination rate of electron-hole pairs. The promising visible-light-driven catalytic activity of the BiOBr-RHC composite makes it a potential candidate for the effective degradation of the antibiotic present in wastewater.

1. Introduction

Pharmaceutical compounds have become a major source of water contamination in recent years owing to their increased consumption and persistence in the environment. Both humans and animals greatly depend on antibiotics as they can cure several diseases caused by bacteria [1]. Tetracycline, fluoroquinolones, sulfonamide, diaminopyrimidines, etc., are popular antibiotics to treat infections. Antibiotics are complex, non-biodegradable substances, and once they are consumed, the body partially metabolizes them, while the unmetabolized parts are discharged through excretion. Even though antibiotics are beneficial, their discharge to the environment can cause severe water and soil pollution [2]. They can easily accumulate in water, and using such polluted water has several adverse effects on the human microbiome, which can result in various health issues, including allergic reactions, chronic toxic effects on the body, and disruptions in the digestive system [3]. Moreover, the presence of antibiotics in waterbodies can lead to the breeding of antibiotic-resistant bacteria, a serious health hazard issue today. The diseases caused by such bacteria cannot be easily cured using presently available antibiotics [4]. The present study focuses on the degradation of NOR, a very common antibiotic used to treat various diseases, including urinary tract infections, gynecological infections, inflammation of the prostate gland, gonorrhea, and bladder infection [5]. NOR is a fluoroquinolone antibiotic, and its presence has been identified in municipal and hospital wastewater as well as in lakes and surface water due to its widespread use. The presence of NOR and other antibiotics in aquatic environments can have adverse ecological effects [6,7]. To maintain a healthy living environment, it is important to remove NOR from water sources through simple and effective approaches. In addition to the removal of various dyes, photocatalysis has emerged as a promising method to degrade the various antibiotics.

To develop visible light-driven catalysts for the degradation of NOR, BiOBr has been utilized. Among bismuth-based photocatalysts, BiOBr has attracted much interest due to its ability to capture visible solar light photons. Bismuth oxybromide is a layered tetragonal phase material with $[Bi_2O_2]^{2+}$ slabs, and Br atoms are bonded via van der Waals interaction. When BiOBr is irradiated with light, photogenerated electrons and holes are formed. However, the faster electron-hole recombination rate limits its application in photocatalysis [8]. To enhance the photocatalytic activity of BiOBr, making a heterojunction structure of

BiOBr with various materials, like TiO_2, Bi_2WO_6, AgBr, or CdS, has been reported [9]. Such an approach facilitates better separation of electron-hole pair and transfer of electrons or holes to the active sites on the heterojunction material [10,11]. It has been also noticed that incorporating carbon materials such as carbon nanotube, graphene oxide, graphitic carbon nitride, carbon quantum dots, etc., into BiOBr facilitates electron transfer as the carbon component can act as an electron acceptor [12,13]. However, preparation of carbonaceous materials either follows a complicated synthesis procedure or involves several chemicals that limit their widespread application. In this context, the development of carbonaceous material via a simple and low-cost approach is very essential. Biochar has gained significant attention as a suitable carbon compound for developing promising composite catalysts for the treatment of wastewater. The addition of biochar helps to promote the better separation of photogenerated electrons and holes, thereby improving its photocatalytic degradation of various pollutants such as dyes, antibiotics, pesticides, and organic compounds present in wastewater [14,15].

In this study, rice husk has been utilized as the material for the production of carbon. Rice husk is a widely available material; approximately 60 billion tons of rice husks are discarded annually worldwide and can be carbonized via a simple approach [16]. To develop a catalysts material capable of degrading the antibiotic, a composite system combining the bismuth oxybromide and rice husk derived carbon was prepared following a simple solid-state method involving the physical mixing and grinding of the precursor materials followed by drying. The incorporation of rice husk-derived carbon into the BiOBr matrix can enhance its photocatalytic efficiency due to its improved charge separation abilities. This study serves as a foundation of the future investigations on the use of biomass derived carbon for developing composite photocatalyst materials for environmental remediation.

2. Characterization

The X-ray diffraction measurements were carried out to explore the phase characteristics of the as-prepared samples by using a Rigaku Mini Flex X-ray diffractometer in the 2θ range of 5–80°. Thermofisher-Nicolet iS50 FTIR spectrometer was used to study the chemical structure of the samples in the wavenumber range of 400 to 4000 cm^{-1}. To further confirm the presence of carbon in the composites, Raman analyses of the samples were carried out with the help of a WITEC Alpha 300 RA–Confocal Raman Microscope. Light absorption properties and band gap of the samples were studied by using an Agilent Carry 5000 UV–visible spectrophotometer in the wavelength range from 200 to 800 nm. The structure and morphology of the samples were investigated using a JOEL-JEM-2100 high-resolution transmission electron microscope (HRTEM) and TESCAN MAIA3 XMH field emission scanning electron microscope (FESEM). The elemental composition of the composite was examined using energy dispersive X-ray spectroscopy (EDS) associated with FESEM. Total organic carbon (TOC) was measured by a total organic carbon analyzer (Vario TOC cube, Elementar, Germany). The surface area, pore volume, and distribution were determined using N_2 adsorption-desorption isotherms obtained using a Quantachrome Nova Touch lx4 Brunauer-Emmett-Teller (BET) Instrument.

3. Experimental

3.1. Materials

All chemical reagents such as bismuth nitrate pentahydrate (Bi $(NO_3)_3.5H_2O$) (98% purity, CAS number: 10035-06-0) and potassium bromide (KBr) (99.99% purity, CAS number: 7758-02-3) were purchased from Sigma Aldrich and were used for the preparation of the photocatalysts. Rice husk was collected from the local rice miller in Kerala, India. Norflox-400 tablet was used for the degradation studies of Norfloxacin, which was marketed by Cipla Ltd and purchased from a local medical shop.

3.2. Synthesis of BiOBr-carbon composite

A solid-state approach was used to synthesize the BiOBr-carbon composites. As obtained, rice husks were washed to remove the contaminants and dried in an oven. The dried rice husks were then heated until they were completely turned black. The resultant black-colored husk was powdered to a fine carbon-rich material (a photograph of the obtained carbon is shown in Fig. 1(a)). For the synthesis of BiOBr-carbon composites, 3.15g of Bi $(NO_3)_3.5H_2O$ and a suitable wt% (say 1, 5, 10, and 20) of rice husk-derived carbon were grinded with the help of a mortar and pestle for a few minutes. To this, 0.95g of KBr was added and grinded until it formed a slurry. The slurry was then dried at a temperature of 90 °C for 6h. The samples with 1, 5, 10 and 20 wt% of RHC were named BiOBr-RHC-1, BiOBr-RHC-5, BiOBr-RHC-10, and BiOBr-RHC-20, respectively. A schematic representation of the synthesis of the BiOBr-RHC composite is depicted in Fig. 1(b).

3.3. Photocatalytic activity

The photocatalytic degradation studies of NOR by BiOBr and BiOBr-RHC composites were conducted under sunlight. For the experiment, 100 mg of the catalyst was dispersed in 50 ml of the NOR solution with a concentration of 10 mg/L and was kept in the dark for 30 min to attain an adsorption-desorption equilibrium. Subsequently, the solution was placed under solar light. During the studies, an intensity of light around 1300×10^2 Lux was recorded with the help of a digital lux meter (LX-101A). At 30-minute intervals, 3 ml of aliquot was collected from the suspension, and the concentration of NOR was estimated using a UV–visible spectrophotometer. In order to determine the degradation efficiency in the presence of the various prepared catalysts, the decrease in absorbance (A) at 273 nm (λ_{max}) of norfloxacin solutions as a function of photo-irradiation time was monitored with the help of an Agilent carry 5000 UV–visible spectrophotometer. In this study, antibiotic-catalyst solutions for degradation studies were prepared in double distilled water. Therefore, before monitoring the absorbance of the antibiotic in the various samples collected at different time intervals, the baseline was corrected by keeping both the reference and sample as water. This initial baseline correction using water will provide only the absorbance data of the antibiotic sample in the subsequent measurements.

The degradation efficiency of the antibiotic in the presence of various catalyst samples at different time intervals was studied from the obtained absorbance data by using the following relation (eqn (1)).

$$\textbf{Percentage of degradation} = (1\text{-}C/C_0)\ x100 \quad (1)$$

where C_0 and C are the concentrations of NOR at initial time t = 0 min (immediately after adding the catalyst) and t min of irradiation. Concentration (C) may be calculated by dividing absorbance (A) by the molar extinction coefficient (ε) of the molecule at that particular wavelength by following the relation, $A = \varepsilon Cl$, where l is the path length of the cuvette (1 cm) used. Thus, the ratio of C/C_0 corresponds to A/A_0, and the degradation efficiency was calculated using eqn (1).

3.4. UPLC-Q-TOF-MS analysis

The chromatographic separation and detection of analytes were carried out by ultra-performance liquid chromatograph coupled to quadrupole time-of-flight mass spectrometer (UPLC-Q-TOF-MS). The Acquity UPLC system is consists of a TUV detector (J12UV750A), a column chamber (J12CHA730G), a quaternary solvent manager (H12QSM632A), and a sample manager FTN (K12SDI069G). Chromatographic separation was achieved using a reverse phase BEH C18

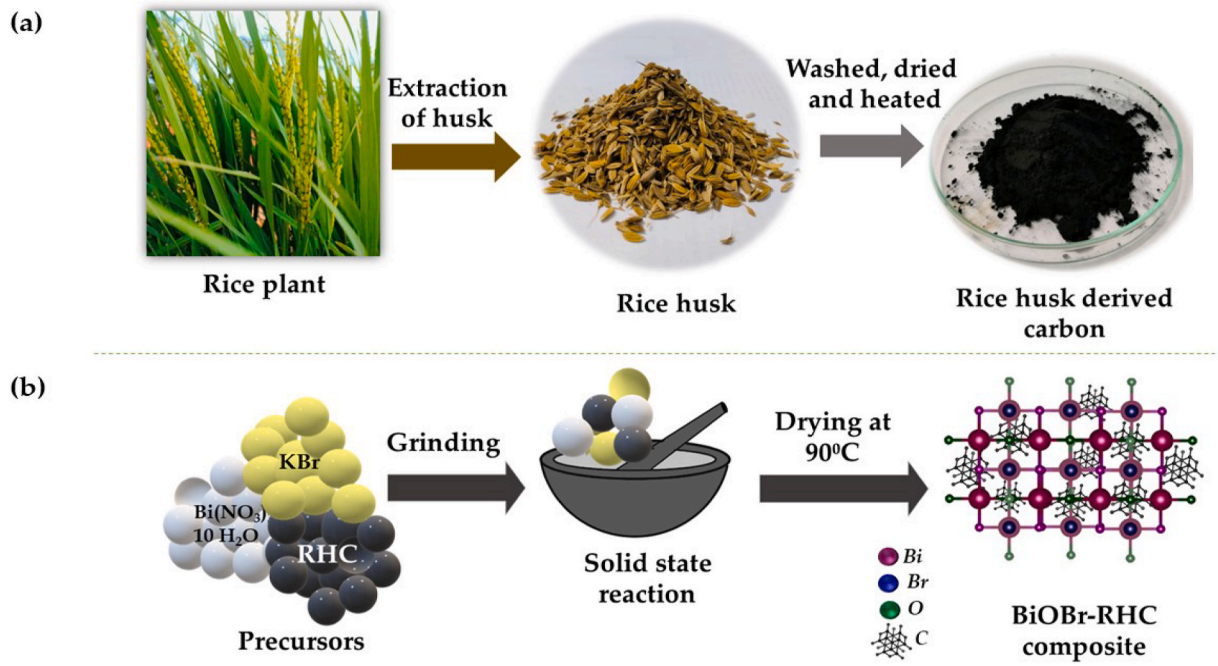

Fig. 1. Schematic presentation of the preparation of (a) RHC and (b) BiOBr-RHC composite via a solid-state reaction method.

column with dimensions of 50 mm × 2.1 mm × 1.7 μm and a flow rate of 0.3 ml/min. The mobile phase, employed in gradient mode, consisted of a mixture of water and acetonitrile with 0.1% formic acid. The total run time was 10 min. The UHPLC system was linked to the Waters Xevo G2 Q-TOF mass spectrometer, equipped with an electrospray ionization (ESI) interface operating in positive and negative ionization modes. The injection volume was set at 10 μL. All samples were examined using the ESI negative ionization mode, scanning the *m/z* range between 50 and 1000. The mass spectra were acquired with collision energy ranging from 5 to 30 eV.

4. Results and discussion

4.1. X-ray diffraction studies

The X-ray Diffraction (XRD) studies were used to determine the phase characteristics and structure of the as-prepared samples. The broad peak centered at 2θ = 21.9° in Fig. 2(a) is the characteristic peak of carbon materials, which is due to the diffraction from the (002) plane of carbon [17]. The diffraction pattern of BiOBr thus obtained (Fig. 2(b)) can be indexed according to the tetragonal phase of BiOBr (JCPDS Card No:73–2061). The intense diffraction peaks were observed in the XRD pattern of BiOBr at 10.9, 21.9, 31.7, 44.7, and 50.5° corresponding to (001), (002), (012), (004), and (104) planes, respectively of the tetragonal BiOBr. In the XRD pattern of BiOBr-RHC composites, all the diffraction peaks from the BiOBr were noticed [18,19]. However, the characteristic peak of carbon was not observed in the pattern of the composites, which might be due to the low weight percentage of RHC in the composites compared to the BiOBr phase [20–22].

4.2. Fourier Transform Infra-Red spectroscopy

FTIR spectroscopy is used to investigate the functional groups and chemical bonding present in the BiOBr, RHC, and BiOBr-RHC

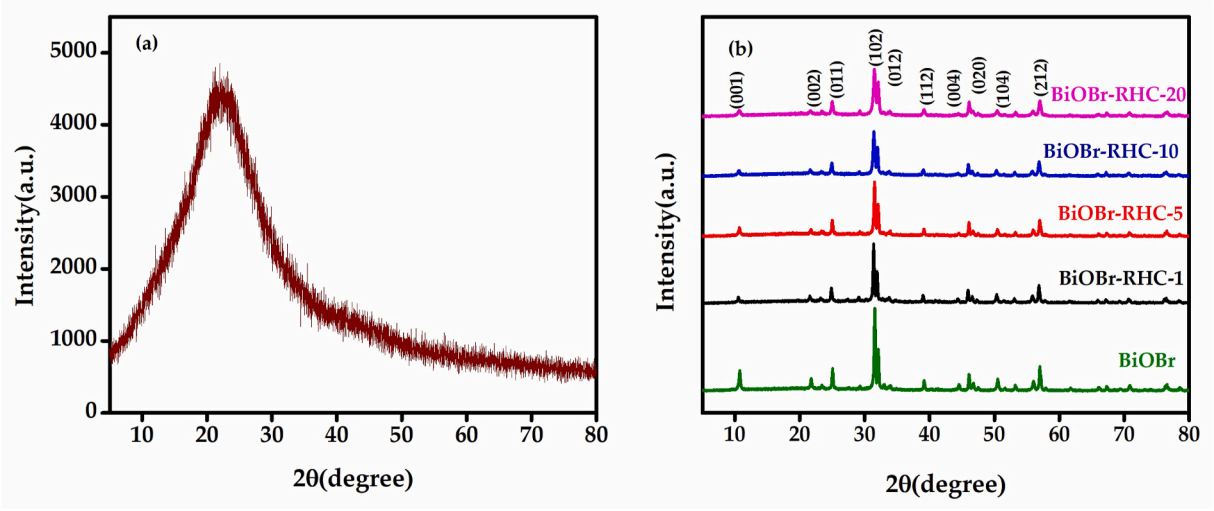

Fig. 2. X-ray diffraction pattern of (a)RHC and (b)BiOBr-RHC composites (different wt% of carbon).

composites (Fig. 3). The bands observed at 1111 and 1623 cm^{-1} indicate the presence of C–O and C═C bonds, which can be associated with carboxyl groups or aromatic structures in the RHC sample. The broad band at 3400 cm^{-1} is associated with the O–H bond stretching [16]. The characteristic band centered at 498 cm^{-1} corresponds to the vibrational stretching of Bi–O bonds in the tetragonal BiOBr. Moreover, the band centered at 843 cm^{-1} arises due to the symmetric stretching vibration of Bi–O bonds [23]. The characteristic bands of both BiOBr and RHC were present in the BiOBr-RHC composites.

4.3. Raman spectroscopy analysis

Raman spectroscopy was also used to confirm the presence of carbon in the BiOBr-RHC composites, and the obtained Raman spectrum of the BiOBr is shown in Fig. 4(a). The peak centered at 89 cm^{-1} is associated with the A_{1g} first-order Raman mode of bismuth in the BiOBr sample [24]. The 114 and 160 cm-1 peaks can be assigned to the internal A1g and E1g stretching modes of Bi–Br bonds. The peak observed at 377 cm^{-1} is due to the Bi–O bond vibration [25]. The Raman spectrum of carbon is depicted in Fig. 4(b), which possesses a D band centered at 1366 cm^{-1} and a graphitic G band at 1590 cm^{-1}. The intensity ratio of the D band to the G band (I_D/I_G) is often used to measure the crystallinity or structural disorder in carbon materials. The I_D/I_G ratio of the rice husk-derived carbon is 0.67, suggesting a higher crystallinity of the carbon material derived from rice husk [26]. The Raman spectra of the composites exhibit the vibrational modes of both BiOBr and RHC, and the Raman spectra of BiOBr-RHC composites obtained are shown in Fig. 4(c). In the context of Raman spectroscopy for carbon materials, second-order Raman spectrum often involves the 2D band and its combinations. It appears that in the Raman spectra of BiOBr-RHC-1 and BiOBr-RHC-5 composites, a band around 3000 cm^{-1} is assigned to the second-order harmonic of the 2D band [27,28]. It is evident from Fig. 4 (d) that as the amount of carbon increases from 1 to 20%, the intensity of the peak from the carbon counterpart increases, which also validates the successful incorporation of RHC in the composites.

4.4. UV–visible spectroscopy

The UV–visible diffuse reflectance spectra were utilized to explore the light-absorbing capabilities and to calculate band gap energies of the BiOBr and BiOBr-RHC composites. The UV–visible absorption spectrum of NOR is depicted in Fig. 5 (the chemical structure of NOR is shown in the inset), which exhibits a broad absorption peak at 273 nm, followed by a narrow, broad peak at 323 nm. The absorption peak at 273 nm corresponds to the π-π* transition of C–C bonds, and the absorption peak at 323 nm represents the n-π* transition of C–O bonds [29]. The absorption spectra of BiOBr, RHC and BiOBr-RHC composites are depicted in Fig. 6(a). The absorption edge at 430 nm indicates that the BiOBr sample can absorb visible light photons.

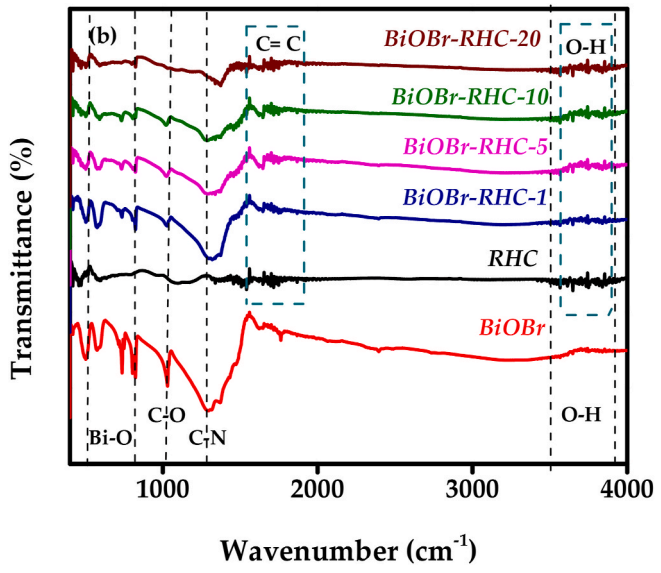

Fig. 3. FTIR spectra of BiOBr, RHC, and BiOBr-RHC composites with different wt% of the carbon.

The photocatalytic activity of a material greatly depends on its band gap because it determines the range of photons that can be absorbed by the material and electron-hole pair formation. Fig. 6(b) shows the Kubelka-Monk plots of BiOBr and BiOBr-RHC composites. The band gap energies of the BiOBr-RHC composites tend to decrease from 2.91 to 2.69eV when the RHC content increases from 1 to 20 wt%.

Mulliken electronegativity theory is typically used to estimate the band edge positions of the conduction band (CB) and valence band (VB) based on electronegativity values. According to the theory, the energy values of the VB and CB of the material can be calculated using eqns (2) and (3).

$$E_{VB} = \chi - E_C + 0.5E_g \quad (2)$$

$$E_{CB} = E_{VB} - E_g \quad (3)$$

Where E_{CB} and E_{VB} are the bandgap potentials of the conduction and valence bands, respectively, χ represents the absolute electronegativity value, and its value is 6.18eV for BiOBr [30–32]. The standard hydrogen electrode potential E_C is ≈ 4.5eV, and the band gap (E_g) of the BiOBr obtained from the Kubelka Munk plots is 2.91eV [33]. On substituting these values in eqs (2) and (3), the conduction and valence band potentials of the BiOBr were found to be 0.23 eV and 3.13 eV, respectively.

4.5. Morphological and Elemental analyses

The morphology of the as-prepared samples was examined using FESEM and HRTEM studies. Fig. 7(a) shows the FESEM images of pristine BiOBr, composed of agglomerated flake structures. Fig. 7(b) is the FESEM image of carbon derived from rice husk, and Fig. 7(c) is the image of the BiOBr-RHC-10 composite. Fig. 7(d–f) represents the TEM, HRTEM images, and the selected area electron diffraction (SAED) pattern of the BiOBr-RHC-10 composite. Inverse fast fourier transformation (IFFT) images (Fig. 7(g) and (h)) were used to obtain a better lattice spacing for both BiOBr and RHC phases in the BiOBr-RHC-10 composite. The inverse FFT pattern of the marked region (in Fig. 7(e)) of the BiOBr-RHC-10 sample shows the presence of two distinct lattice planes with d-spacings of 0.27 and 0.24 nm corresponding to (110) and (002) planes of BiOBr and RHC, respectively [34]. The SAED pattern of the BiOBr-RHC-10 shown in the inset of Fig. 7(e) indicates the polycrystalline nature of the composite.

EDS measurement was carried out using the BiOBr-RHC-10 sample, and the spectrum of the sample is shown in Fig. 8. The recorded EDS profile confirms the presence of elements, such as Bi, O, Br, and C, in the sample.

4.6. BET analysis

The N_2 adsorption–desorption isotherms and the pore size distributions of the BiOBr, RHC, and BiOBr-RHC-10 are depicted in Fig. 9. The BiOBr, RHC and BiOBr-RHC-10 composites have specific surface areas (S_{BET}) of 1.09, 8.09, and 1.91 m^2g^{-1} and corresponding total pore volume (at $p/p_0 = 0.99$) noticed for the samples are 0.011, 0.016 and 0.008 cm^3/g, respectively.

4.7. Photocatalytic degradation studies of pharmaceutical pollutant

4.7.1. Photocatalytic degradation of NOR

The photocatalytic degradation of NOR under visible light was

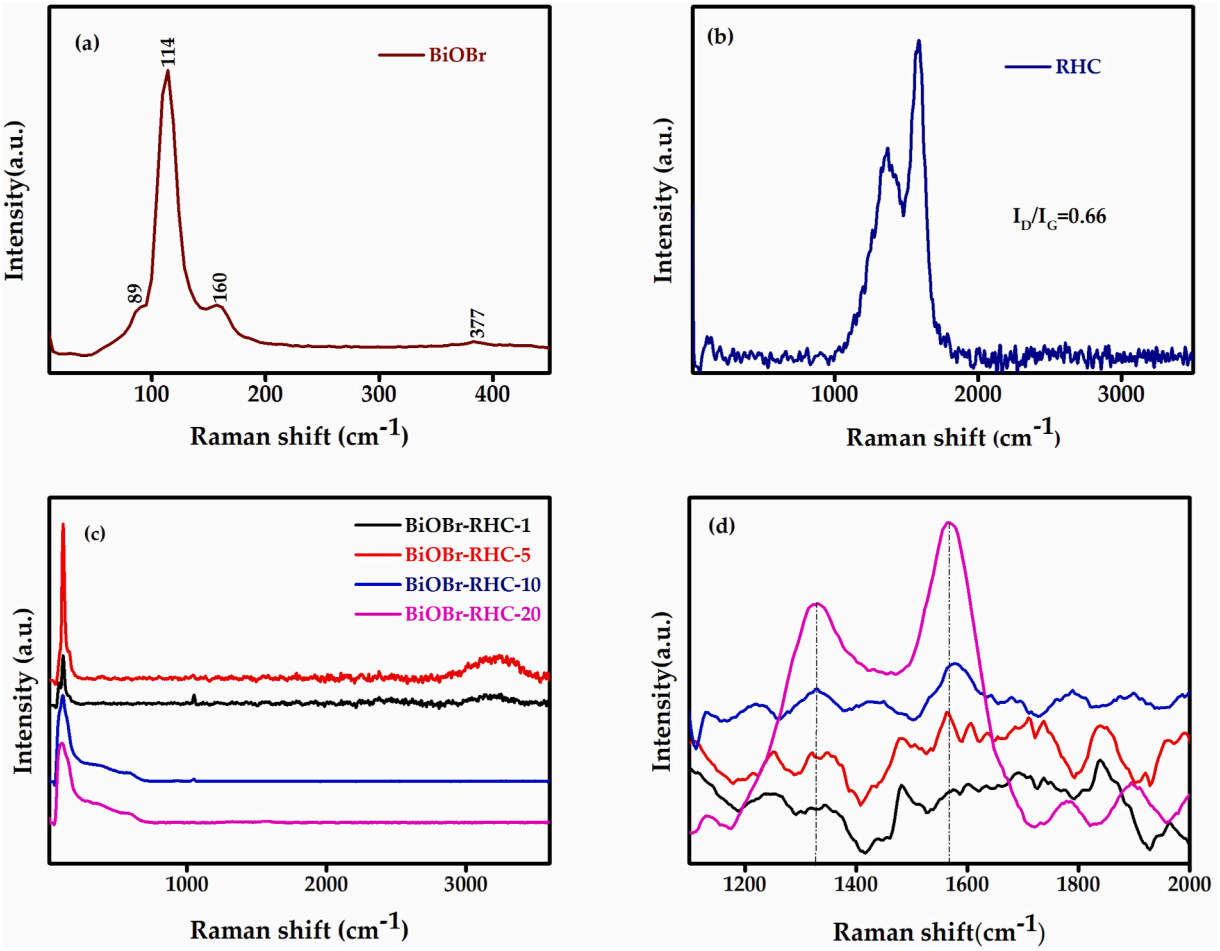

Fig. 4. Raman spectra of (a)BiOBr, (b)RHC, and (c)BiOBr-RHC composites with different wt% of carbon (d) portion of the spectra of BiOBr-RHC composites from 1200 to 2000 cm^{-1}.

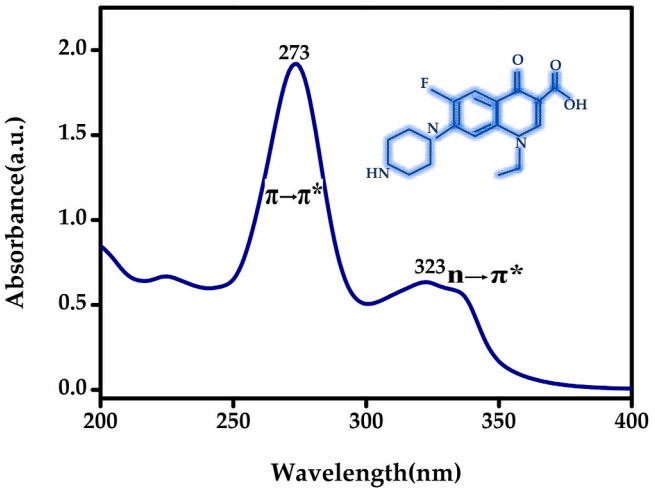

Fig. 5. UV–Visible spectrum of Norfloxacin.

studied using BiOBr and BiOBr-RHC composites as the catalysts and the obtained C/C_0 plots are shown in Fig. 10(a). The degradation of NOR in the BiOBr-RHC composites is assessed spectrophotometrically by monitoring the decrease in absorbance value at 273 nm. Observed NOR removal efficiency of various composite catalysts in 3h is in the order: BiOBr-RHC-10 (93%) > BiOBr-RHC-1 (75%) ~ BiOBr-RHC-5 (75%) > pristine BiOBr (73%) > BiOBr-RHC-20 (32%). It appears that the degradation behavior of BiOBr-RHC-5 and BiOBr-RHC-1 is close to that of pristine BiOBr. The study reveals that incorporating RHC into BiOBr materials enhanced its visible-light-driven photocatalytic activity towards the degradation of NOR. However, it has been noticed that the photodegradability of the composite materials decreased when the RHC content was increased from 10 to 20 wt% in BiOBr-RHC composite. The excessive use of RHC in the BiOBr composite can mask the BiOBr particles, which can reduce the formation of photogenerated electron-hole pairs in BiOBr, and this may presumably be the reason for the observed reduction in the photodegradation ability of the BiOBr-RHC composite at higher RHC loading [35]. The results of the study indicate that the optimum amount of RHC for showing better catalytic reduction of NOR is 10 wt%. The degradation kinetics of NOR is well fitted to the first order pseudo kinetic equation (eqn (4)), and the ($-ln\ C/C_0$) versus irradiation time curve of the different catalysts is provided in Fig. 10(b).

$$(-ln\ C/C_0) = kt \tag{4}$$

C_0 and C are NOR concentrations at time t=0 min and t min and k is the rate constant. It can be noticed from Fig. 10(b) that the BiOBr-RHC-10 composite exhibits the highest rate constant value of 0.01123 min^{-1}. Studies further confirm that BiOBr-RHC-10 composite is a promising catalyst material for NOR degradation under visible light irradiation and a degradation efficacy of 93% can be achieved towards NOR in 180 min. The optimum introduction of RHC into BiOBr can effectively promote the separation efficiency of electron-hole pairs and improve photocatalytic performances.

A comparative study of the photocatalytic performance of the BiOBr-

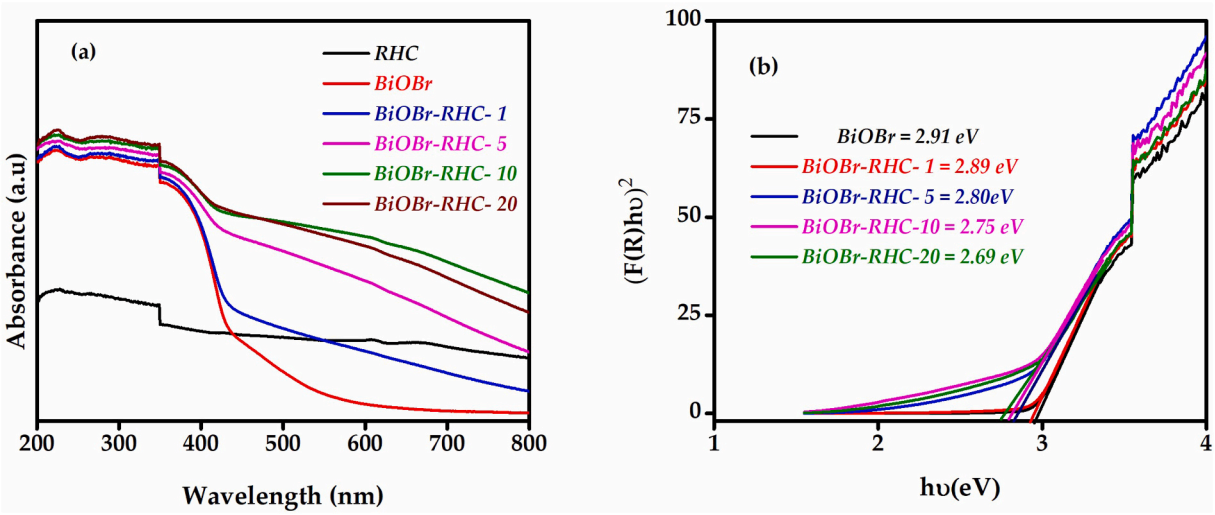

Fig. 6. UV–Visible spectra of (a) BiOBr, RHC, and BiOBr-RHC composites with different wt% of carbon (b)Kubelka-monk plot showing the band gap energies of the BiOBr and BiOBr-RHC composites.

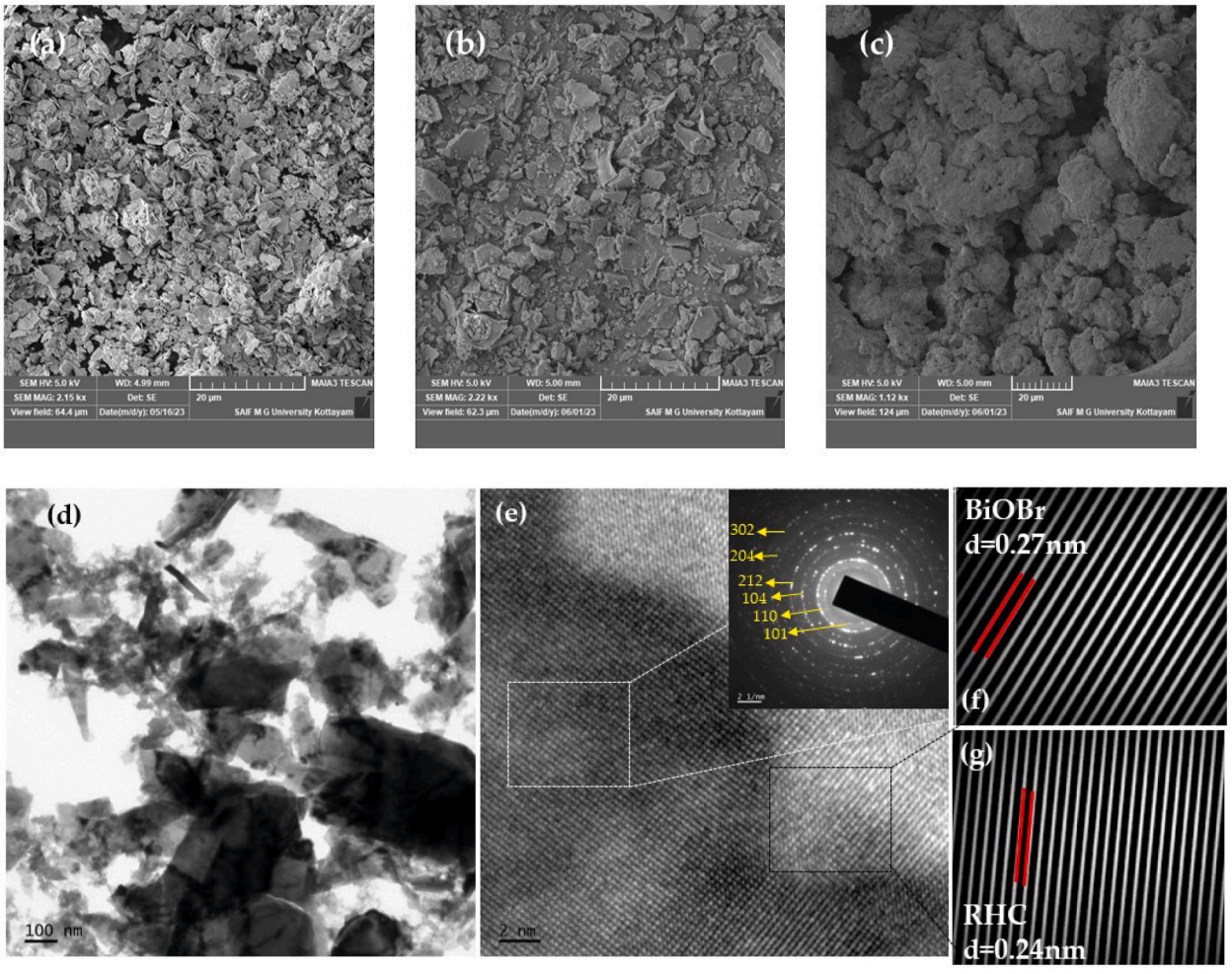

Fig. 7. FESEM images of (a)BiOBr (b)RHC (c)BiOBr-RHC-10 (d) TEM image (e)HRTEM image with the SAED pattern of BiOBr-RHC-10 in inset, (f) and (g) IFFT images of BiOBr and RHC.

RHC composite towards the degradation of NOR removal and that of a few other previously reported photocatalysts are presented in Table 1. The comparison with other previously reported photocatalysts indicates that the BiOBr-RHC composite is a suitable photocatalytic material for NOR degradation, making it a promising candidate for applications in wastewater treatment.

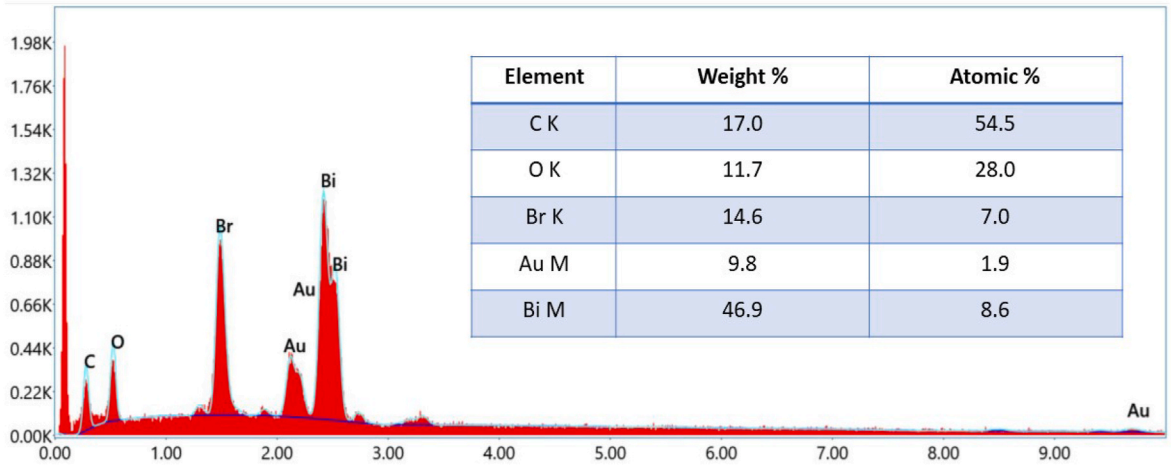

Element	Weight %	Atomic %
C K	17.0	54.5
O K	11.7	28.0
Br K	14.6	7.0
Au M	9.8	1.9
Bi M	46.9	8.6

Fig. 8. EDS spectra of BiOBr-RHC-10 composite.

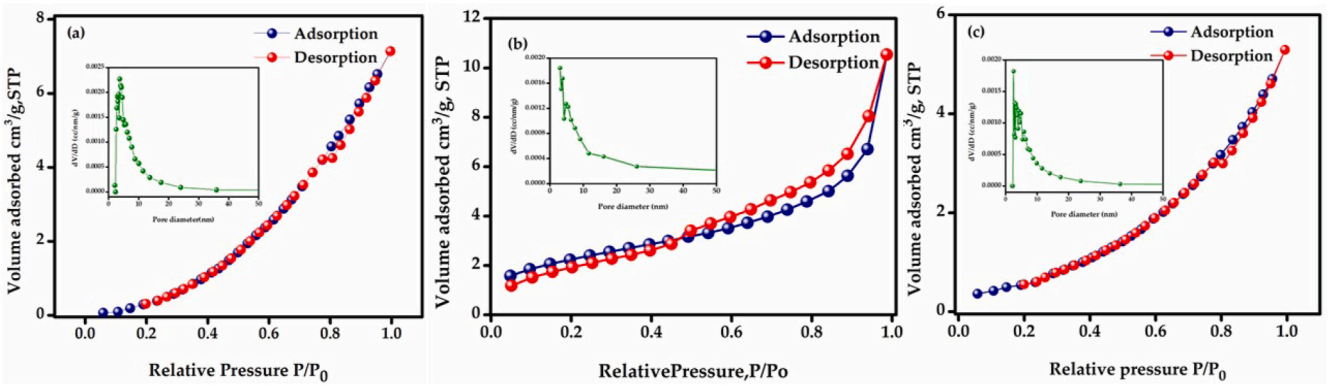

Fig. 9. (a) N_2 adsorption-desorption isotherms and the inset shows the corresponding pore size distribution of the (a)BiOBr (b)RHC (c)BiOBr-RHC-10 composite.

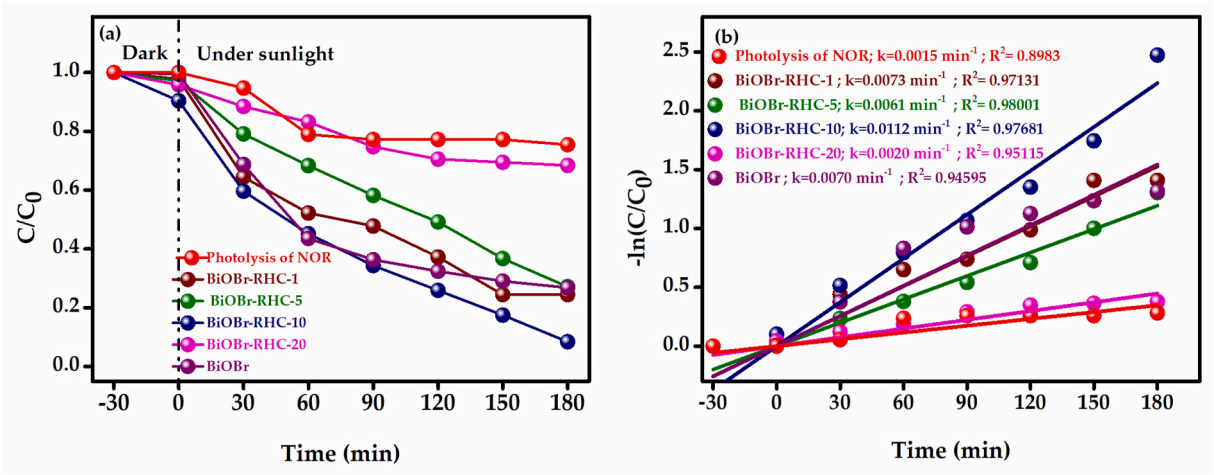

Fig. 10. (a)Photocatalytic degradation curves of NOR (b) the kinetic plot of NOR degradation with different photocatalysts under visible light irradiation.

4.7.2. Cycle test

The stability of a catalyst is crucial for long-term application. However, photo-corrosion or photo-dissolution during photocatalytic reactions can lead to a reduction in photocatalytic activity. To assess the stability and reusability of BiOBr-RHC-10, recycle tests were conducted using NOR and the XRD patterns of BiOBr-RHC-10 before and after the tests were also examined. The results, as depicted in Fig. 11(a), reveal a slight decrease in the photocatalytic activity of the BiOBr-RHC photocatalyst throughout four cycles. This decrease in degradation efficiency is likely to be attributed to the inevitable loss of the catalyst during the experimental process [42]. Additionally, the XRD results in Fig. 11(b) demonstrate no noticeable change peak in the XRD pattern of the sample after four cycles. The crystal structure of BiOBr-RHC-10 after four cycles remains well-maintained, suggesting excellent stability of BiOBr-RHC-10 even after repeated use.

Table 1
Comparison of the performance of BiOBr-RHC composite with other promising photocatalysts for NOR degradation.

Sl. No	Photocatalyst	NOR concentration	Light sources	Degradation efficiency	References
1.	rGO/Bi_2WO_6	10 ppm	300W Xenon lamp	87.49 % 180min	[36]
2.	Fe_3O_4/ MWCNTs + H_2O_2 (Fenton process)	0.5 mg/mL	300W Xenon lamp	91.36% 180 min	[37]
3.	CdS/BiOBr	10 mg/L	15W Panasonic cool daylight lamp	100% 240 min	[38]
4.	TiO_{2-x} polymorphs	0.1 mg/L	300 W Xe lamp 400 nm with cut-on filter	100% 240 min	[39]
5.	RGO-ZnS	20 mg/L	300W Hg vapor lamp	92% 360min	[40]
6.	AgI/SnO2	20 ppm	Xenon lamp400 nm with cut-on filter	100% 300 min	[41]
7.	**BiOBr-RHC**	**10 mg/L**	**Sunlight**	**93% 180 min**	**This work**

4.7.3. Analysis of NOR photodegradation intermediates and mineralization pathways

TOC analysis was used to assess the degree of mineralization, as shown in Fig. 12. The results indicate that on sunlight exposure of 180 min, the mineralization percentage reached 57%. The observed percentage of TOC in comparison with degradation efficiency (C/C_0) may be attributed to the higher stability of the NOR molecule with its aromatic ring structure having extended delocalized π-electrons. Additionally, generating numerous intermediate products during the degradation process could still contribute to the TOC of the solution [43].

By assessing the mass-to-charge ratio (m/z) of the molecular ion peak, it is possible to determine the relative molecular mass. Mass spectrometry serves as a method to ascertain the relative molecular mass of unidentified substances. The UPLC/Q-TOF/MS results can provide the molecular weight of degradation products. The structure of Norfloxacin ($C_{16}H_{18}FN_3O_3$) comprises a piperazine ring and a quinoline ring, with the side chain consisting of carboxyl, ethyl, and fluorine atoms with m/z value of 320 [44]. The fragmented product with a protonated form of m/z value of 350 ($C_{16}H_{17}FN_3O_5$) was observed. Subsequent products with m/z values of 322 ($C_{15}H_{17}FN_3O_4$), 279 ($C_{13}H_{12}FN_2O_4$), and 251 ($C_{12}H_{12}N_2O_3$), were probably resulted from the partial elimination of –CO, $–C_2H_5N$, –CO respectively. Additionally, another product with a protonated m/z of 304 ($C_{15}H_{14}N_3O_3$) was also present, attributed to the dehydroxylated form of NOR [39,45].

4.7.4. Reactive species and possible mechanism

Different reactive species role in NOR degradation is validated with the help of scavenger studies, and the obtained C/C_0 plots thus obtained are shown Fig. 13(a). To perform the scavenger studies, isopropyl alcohol (IPA), *p*-benzoquinone (BQ), dimethyl sulfoxide (DMSO), and ethylene diamine tetra acetic acid (EDTA) were added to the NOR BiOBr-RHC-10 solution as scavengers for hydroxyl radical, oxide radical, electrons, and holes, respectively. The percentage of degradation NOR in 180 min in the presence of various scavengers are presented in Fig. 13 (b). Degradation efficiency is considerably reduced in the presence of EDTA and BQ, which reveals that both holes and oxide radicals are the active species involved in the degradation of NOR when BiOBr-RHC is used as the catalyst. Feng Cao et al. al noticed similar behavior of hole and oxide radicals as the active species in the degradation of antibiotics in water [46].

When NOR solution containing BiOBr-RHC composites was exposed to light, the photogenerated electrons-holes were formed as provided in

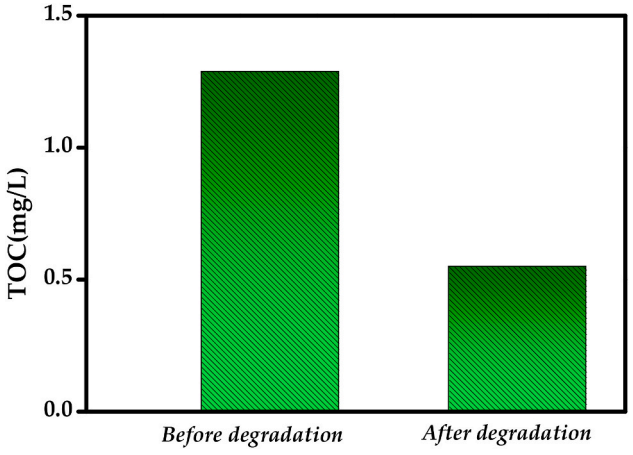

Fig. 12. TOC removal of NOR.

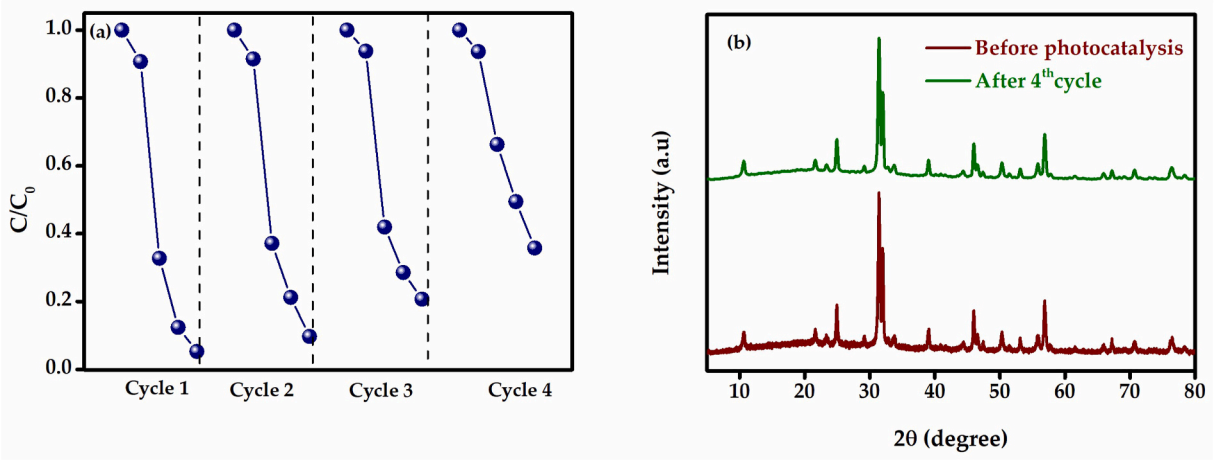

Fig. 11(a). Four cycles of NOR degradation and (b) XRD pattern before and after four cycles of NOR degradation for BiOBr-RHC-10.

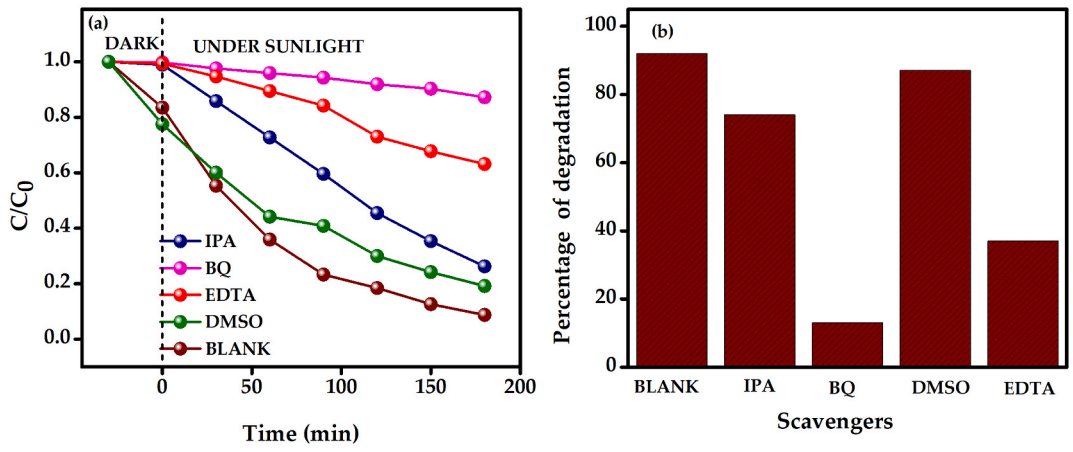

Fig. 13. (a) C/C_0 curves of BiOBr-RHC-10 composite and (b) the degradation percentage in radical scavenging experiments.

eqn (5). These photogenerated electrons in the CB of the composite are likely to transfer to the surface of RHC because they can act as an electron acceptor (eq (6)). The transferred electrons (e^-) from the conduction band of BiOBr can participate in the reduction reactions. As given in eq (7), these electrons can reduce oxygen molecules (O_2) to form superoxide radicals (O_2^-). Simultaneously, holes (h^+) are formed in the valence band of BiOBr (eq (5)) and can react with water molecules (H2O) to generate hydroxyl radicals (OH.), and it is provided in eq (8). The superoxide radicals (O_2^-) and positive holes (h^+) can react with NOR molecules given in eq (9) and undergo a series of oxidation reactions, resulting in the degradation of NOR into carbon dioxide (CO_2), water (H_2O), and small byproducts. The introduction of RHC also allows NOR molecules to be adsorbed on its surface and facilitates a fast electron transfer path [35,47]. A schematic illustration showing the possible mechanism of the photocatalytic degradation of NOR by BiOBr-RHC composites is given in Fig. 14.

$$BiOBr\text{–}RHC + h\upsilon \rightarrow (e^-_{CB} + h^+_{VB}) \quad (5)$$

$$BiOBr\ (e^-_{CB}) \rightarrow RHC(e^-_{CB}) \quad (6)$$

$$e^- + O_2 \rightarrow O_2^- \quad (7)$$

$$h^+ + H_2O \rightarrow H^+ + OH \quad (8)$$

$$h^+ + O_2 \rightarrow CO_2 + H_2O + \text{small byproducts} \quad (9)$$

5. Conclusion

In summary, BiOBr-RHC composites were prepared via a solid-state reaction method, and the photocatalytic degradation studies of NOR and the mechanisms involved were investigated. The phase characteristics and crystallinity, chemical bonding, and light absorption properties of the as-developed composites were studied using XRD, FTIR, and UV–visible spectroscopy, respectively. Raman spectroscopic analysis confirmed the presence of the carbon in the composites. The composite of BiOBr-RHC with 10 wt% of carbon shows improved photocatalytic degradation of NOR (93% in 180 min) under visible light irradiation. The involvement of reactive species in the reaction was determined through radical scavenger experiments, revealing that hole and oxide radicals played a more prominent role. The intermediate products of norfloxacin degradation were identified via UPLC/Q-TOF/MS analysis. The introduction of rice husk-derived carbon provides better separation and transfer of electron-hole pairs that can enhance better photocatalytic activity. The studies confirm that BiOBr-RHC composites can

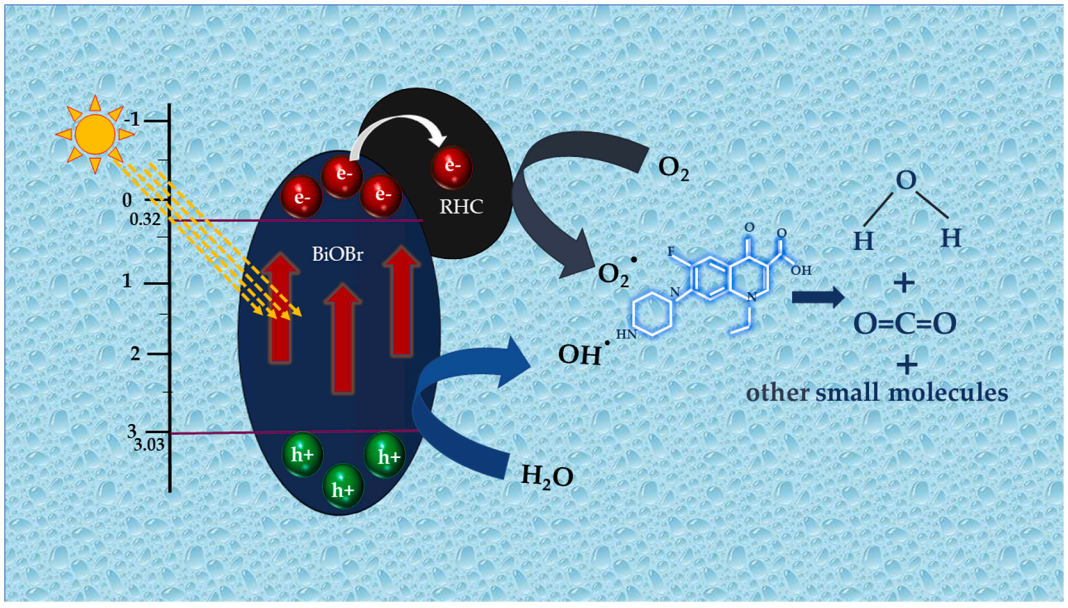

Fig. 14. Schematic representation of the photocatalytic degradation of NOR by BiOBr-RHC composite.

be considered a promising photocatalyst for the efficient degradation of NOR pollutants from water.

CRediT authorship contribution statement

Bosely Anne Bose: Writing – original draft, Methodology, Investigation, Formal analysis, Data curation, Conceptualization. **Ange Nzihou:** Writing – review & editing. **Daniel Thangadurai:** Writing – review & editing, Resources. **Abhijit Saha:** Writing – review & editing, Supervision, Funding acquisition. **Nandakumar Kalarikkal:** Writing – review & editing, Supervision, Resources, Conceptualization.

Declaration of competing interest

The authors declare the following financial interests/personal relationships which may be considered as potential competing interests:

Prof. (Dr.) Nandakumar Kalarikkal reports financial support was provided by University Grants Commission Department of Atomic Energy Consortium for Scientific Research Kolkata Centre. If there are other authors, they declare that they have no known competing financial interests or personal relationships that could have appeared to influence the work reported in this paper.

Data availability

The authors do not have permission to share data.

Acknowledgment

The authors would like to acknowledge the financial support from the CRS program of UGC-DAE CSR, Kolkata Centre (UGC-DAE-CSR-KC/CRS/19/RC08/0485), India. The author NK acknowledges SERB: CRG (Grant No. CRG/2021/001506), UGC-Govt. of India for funding through the Innovative Program and Special Assistance Program (SAP Grant Nos. F.530/12/DRS/2009; F.530/13/DRS II/2016), UGC: Scheme for Promotion of Academic and Research Collaboration (SPARC Grant Nos. P930, P1400, P1429, P1460) supported by MHRD, Govt. of India, DST: Nano Mission (Grant No. SR/NM/NS-1420-2014(C)), DST: Fund for Improvement of S&T Infrastructure (FIST Grant No. SR/FST/P SI-143/2009), DAE-Board of Research in Nuclear Sciences (BRNS Grant No. 39/29/2015-BRNS/39009), and DST Promotion of University Research and Scientific Excellence (PURSE Grant No. SR/S9/Z-23/2010/22(C, G)), Government of India programs for providing the facilities for research and development in IIUCNN, MGU. The author NK also acknowledges CEFIPRA (Project 6408-1) scheme and Rashtriya Uchchatar Shiksha Abhiyan (RUSA) 2.0 Scheme, Ministry of Education-Govt. of India for funding. The authors NK and BAB express gratitude to Mr. Anu A.S, Analytical Engineer, IIUCNN, MGU, for the HRTEM imaging, Mr. Cyrus Koshy, IUIC, for UPLC analysis, SES, CUSAT, for TOC analysis and SAIF, MGU, for the Raman FESEM and the EDS analyses, CLIF, University of Kerala, Govt College,Vazuthacad for BET analysis.

References

[1] N. Askari, M. Beheshti, D. Mowla, M. Farhadian, Facile construction of novel Z-scheme MnWO4/Bi2S3 heterojunction with enhanced photocatalytic degradation of antibiotics, Mater. Sci. Semicond. Process. 127 (2021) 105723, https://doi.org/10.1016/j.mssp.2021.105723.

[2] T. Senasu, T. Chankhanittha, K. Hemavibool, S. Nanan, Visible-light-responsive photocatalyst based on ZnO/CdS nanocomposite for photodegradation of reactive red azo dye and ofloxacin antibiotic, Mater. Sci. Semicond. Process. 123 (2021) 105558, https://doi.org/10.1016/j.mssp.2020.105558.

[3] S.I. Polianciuc, A.E. Gurzău, B. Kiss, M. Georgia Ștefan, F. Loghin, Antibiotics in the environment: causes and consequences, Med, Pharm. Reports. 93 (2020) 231–240, https://doi.org/10.15386/mpr-1742.

[4] K. Qin, Q. Zhao, H. Yu, X. Xia, J. Li, S. He, L. Wei, T. An, A review of bismuth-based photocatalysts for antibiotic degradation: insight into the photocatalytic degradation performance, pathways and relevant mechanisms, Environ. Res. 199 (2021) 111360, https://doi.org/10.1016/j.envres.2021.111360.

[5] K. Kanagamani, P. Muthukrishnan, K. Shankar, A. Kathiresan, H. Barabadi, M. Saravanan, Antimicrobial, Cytotoxicity and photocatalytic degradation of norfloxacin using Kleinia grandiflora mediated Silver nanoparticles, J. Clust. Sci. 30 (2019) 1415–1424, https://doi.org/10.1007/s10876-019-01583-y.

[6] X. Jin, X. Zhou, P. Sun, S. Lin, W. Cao, Z. Li, W. Liu, Photocatalytic degradation of norfloxacin using N-doped TiO2: Optimization, mechanism, identification of intermediates and toxicity evaluation, Chemosphere 237 (2019), https://doi.org/10.1016/j.chemosphere.2019.124433.

[7] N. Yin, H. Chen, X. Yuan, Y. Zhang, M. Zhang, J. Guo, Y. Zhang, L. Qiao, M. Liu, K. Song, Highly efficient photocatalytic degradation of norfloxacin via Bi2Sn2O7/PDIH Z-scheme heterojunction: influence and mechanism, J. Hazard Mater. 436 (2022) 129317, https://doi.org/10.1016/j.jhazmat.2022.129317.

[8] T. Senasu, S. Nijpanich, S. Juabrum, N. Chanlek, S. Nanan, CdS/BiOBr heterojunction photocatalyst with high performance for solar-light-driven degradation of ciprofloxacin and norfloxacin antibiotics, Appl. Surf. Sci. 567 (2021) 150850, https://doi.org/10.1016/j.apsusc.2021.150850.

[9] Q. Wang, D. Jiao, J. Lian, Q. Ma, J. Yu, H. Huang, J. Zhong, J. Li, Preparation of efficient visible-light-driven BiOBr/Bi2O3 heterojunction composite with enhanced photocatalytic activities, J. Alloys Compd. 649 (2015) 474–482, https://doi.org/10.1016/j.jallcom.2015.07.126.

[10] S. Kappadan, S. Thomas, N. Kalarikkal, Enhanced photocatalytic performance of BaTiO3/g-C3N4 heterojunction for the degradation of organic pollutants, Chem. Phys. Lett. 771 (2021) 138513, https://doi.org/10.1016/j.cplett.2021.138513.

[11] S. Kappadan, S. Thomas, N. Kalarikkal, BaTiO3/ZnO heterostructured photocatalyst with improved efficiency in dye degradation, Mater. Chem. Phys. 255 (2020) 123583, https://doi.org/10.1016/j.matchemphys.2020.123583.

[12] X. Tu, S. Luo, G. Chen, J. Li, One-pot synthesis, characterization, and enhanced photocatalytic activity of a BiOBr–graphene composite, Chem. Eur J. 18 (2012) 14359–14366, https://doi.org/10.1002/chem.201200892.

[13] J. Ge, Y. Zhang, S.J. Park, Recent advances in carbonaceous photocatalysts with enhanced photocatalytic performances: a mini-review, Materials 12 (2019), https://doi.org/10.3390/ma12121916.

[14] G. Rangarajan, A. Jayaseelan, R. Farnood, Photocatalytic reactive oxygen species generation and their mechanisms of action in pollutant removal with biochar supported photocatalysts: a review, J. Clean. Prod. 346 (2022) 131155, https://doi.org/10.1016/j.jclepro.2022.131155.

[15] Y. Lu, Y. Cai, S. Zhang, L. Zhuang, B. Hu, S. Wang, J. Chen, X. Wang, Application of biochar-based photocatalysts for adsorption-(photo)degradation/reduction of environmental contaminants: mechanism, challenges and perspective, Biochar 4 (2022), https://doi.org/10.1007/s42773-022-00173-y.

[16] M. Liu, L. Guan, Y. Wen, L. Su, Z. Hu, Z. Peng, S. Li, Q. Tang, Z. Zhou, N. Zhou, Rice husk biochar mediated red phosphorus for photocatalysis and photothermal removal of E. coli, Food Chem. 410 (2023), https://doi.org/10.1016/j.foodchem.2023.135455.

[17] P. Bhavani, D. Praveen Kumar, M. Hussain, T.M. Aminabhavi, Y.K. Park, Eco-friendly rice husk derived biochar as a highly efficient noble Metal-Free cocatalyst for high production of H2 using solar light irradiation, Chem. Eng. J. 434 (2022) 134743, https://doi.org/10.1016/j.cej.2022.134743.

[18] T.M. Project, Materials Data on BiBrO by Materials Project, (n.d.). https://doi.org/https://doi.org/10.17188/1199215.

[19] T.M. Project, Materials Data on carbon by Materials Project, (n.d.). https://doi.org/10.17188/1208406.

[20] S. Qu, Y. Xiong, J. Zhang, Graphene oxide and carbon nanodots co-modified BiOBr nanocomposites with enhanced photocatalytic 4-chlorophenol degradation and mechanism insight, J. Colloid Interface Sci. 527 (2018) 78–86, https://doi.org/10.1016/j.jcis.2018.05.038.

[21] Z. Jiang, F. Yang, G. Yang, L. Kong, M.O. Jones, T. Xiao, P.P. Edwards, The hydrothermal synthesis of BiOBr flakes for visible-light-responsive photocatalytic degradation of methyl orange, Journal Photochem. Photobiol. A Chem. 212 (2010) 8–13, https://doi.org/10.1016/j.jphotochem.2010.03.004.

[22] L. Allagui, B. Chouchene, T. Gries, G. Medjahdi, E. Girot, X. Framboisier, A.B. haj Amara, L. Balan, R. Schneider, Core/shell rGO/BiOBr particles with visible photocatalytic activity towards water pollutants, Appl. Surf. Sci. 490 (2019) 580–591, https://doi.org/10.1016/j.apsusc.2019.06.091.

[23] S.T. Navale, Q. Huang, P. Cao, V.B. Patil, F.J. Stadler, C2H5OH sensing properties of solid-state mediated BiOBr nanoplates, Sensors Actuators, B Chem 300 (2019), https://doi.org/10.1016/j.snb.2019.126987.

[24] K. Trentelman, A note on the characterization of bismuth black by Raman microspectroscopy, J. Raman Spectrosc. 40 (2009) 585–589, https://doi.org/10.1002/jrs.2184.

[25] D. Wu, S. Yue, W. Wang, T. An, G. Li, L. Ye, H.Y. Yip, P.K. Wong, Influence of photoinduced Bi-related self-doping on the photocatalytic activity of BiOBr nanosheets, Appl. Surf. Sci. 391 (2017) 516–524, https://doi.org/10.1016/j.apsusc.2016.05.144.

[26] S.K. Sharma, G. Sharma, A. Sharma, K. Bhardwaj, K. Preeti, K. Singh, A. Kumar, V. K. Pal, E.H. Choi, S.P. Singh, N.K. Kaushik, Synthesis of silica and carbon-based nanomaterials from rice husk ash by ambient fiery and furnace sweltering using a chemical method, Appl. Surf. Sci. Adv. 8 (2022) 100225, https://doi.org/10.1016/j.apsadv.2022.100225.

[27] L. Bokobza, J.-L. Bruneel, M. Couzi, Raman Spectra of Carbon-Based Materials (From Graphite to Carbon Black) and of Some Silicone Composites, C, vol. 1, 2015, pp. 77–94, https://doi.org/10.3390/c1010077.

[28] A.C. Ferrari, D.M. Basko, Raman spectroscopy as a versatile tool for studying the properties of graphene, Nat. Nanotechnol. 8 (2013) 235–246, https://doi.org/10.1038/nnano.2013.46.

[29] A.A. Elabd, O.A. Elhefnawy, Uranyl ion assessment based on the fluorescence quenching of Norfloxacin, J. Radioanal. Nucl. Chem. 329 (2021) 935–944, https://doi.org/10.1007/s10967-021-07831-8.
[30] X. Qiu, J. Li, Y. Zhao, S. Lin, Z. Sun, Y. Fang, L. Guo, The formation of Z-scheme AgI/BiOBr heterojunction and its excellent photocatalytic performance, J. Alloys Compd. 967 (2023) 171739, https://doi.org/10.1016/j.jallcom.2023.171739.
[31] X. Zhang, Q. Lu, L. Jian, W. Wei, Z. Zhang, Z. Luo, Y. Zhao, J. Chen, Y. Li, Newly constructed Z-scheme Cu2ZnSnS4/BiOBr heterostructure for high-efficient photocatalytic applications, Colloids Surfaces A Physicochem. Eng. Asp. 663 (2023) 131123, https://doi.org/10.1016/j.colsurfa.2023.131123.
[32] M. Song, M. Li, H. Li, P. Wang, Y. Wu, L. Li, Novel through-holes g-C3N4/BiOBr S-scheme heterojunction: charge relocation mechanism and DFT insights, Surface. Interfac. 41 (2023) 103227, https://doi.org/10.1016/j.surfin.2023.103227.
[33] A. Hussain, J. Hou, M. Tahir, X. Wang, M.U. Qadri, T. Jiang, X. Tu, T. Zhang, Q. Dou, J. Zou, Fine-tuning internal electric field of BiOBr for suppressed charge recombination, J. Environ. Chem. Eng. 9 (2021) 104766, https://doi.org/10.1016/j.jece.2020.104766.
[34] T. Li, Y. Gao, L. Zhang, X. Xing, X. Huang, F. Li, Y. Jin, C. Hu, Enhanced Cr(VI) reduction by direct transfer of photo-generated electrons to Cr 3d orbitals in CrO42-intercalated BiOBr with exposed (110) facets, Appl. Catal. B Environ. 277 (2020) 119065, https://doi.org/10.1016/j.apcatb.2020.119065.
[35] W. Song, J. Zhao, X. Xie, W. Liu, S. Liu, H. Chang, C. Wang, Novel BiOBr by compositing low-cost biochar for efficient ciprofloxacin removal: the synergy of adsorption and photocatalysis on the degradation kinetics and mechanism insight, RSC Adv. 11 (2021) 15369–15379, https://doi.org/10.1039/d1ra00941a.
[36] Y. Zhao, X. Liang, X. Hu, J. Fan, rGO/Bi2WO6 composite as a highly efficient and stable visible-light photocatalyst for norfloxacin degradation in aqueous environment, J. Colloid Interface Sci. 589 (2021) 336–346, https://doi.org/10.1016/j.jcis.2021.01.016.
[37] T. Shi, J. Peng, J. Chen, C. Sun, H. He, Heterogeneous photo-Fenton degradation of norfloxacin with Fe3O4-Multiwalled carbon nanotubes in aqueous solution, Catal. Letters. 147 (2017) 1598–1607, https://doi.org/10.1007/s10562-017-2026-4.
[38] T. Senasu, S. Nijpanich, S. Juabrum, N. Chanlek, S. Nanan, CdS/BiOBr heterojunction photocatalyst with high performance for solar-light-driven degradation of ciprofloxacin and norfloxacin antibiotics, Appl. Surf. Sci. 567 (2021) 150850, https://doi.org/10.1016/j.apsusc.2021.150850.
[39] H. Yang, L. Mei, P. Wang, J. Genereux, Y. Wang, B. Yi, C. Au, L. Dang, P. Feng, Photocatalytic degradation of norfloxacin on different TiO 2−X polymorphs under visible light in water, RSC Adv. 7 (2017) 45721–45732, https://doi.org/10.1039/C7RA09022F.
[40] J. Bai, Y. Li, P. Jin, J. Wang, L. Liu, Facile preparation 3D ZnS nanospheres-reduced graphene oxide composites for enhanced photodegradation of norfloxacin, J. Alloys Compd. 729 (2017) 809–815, https://doi.org/10.1016/j.jallcom.2017.07.057.
[41] A.A. Baoum, M.S. Amin, R.M. Mohamed, Decoration of SnO2 nanosheets by AgI nanoparticles driven visible light for norfloxacin degradation, Appl. Nanosci. 8 (2018) 2093–2102, https://doi.org/10.1007/s13204-018-0890-x.
[42] J. Wang, W. Liu, D. Zhong, Y. Ma, Q. Ma, Z. Wang, J. Pan, Fabrication of bismuth titanate nanosheets with tunable crystal facets for photocatalytic degradation of antibiotic, J. Mater. Sci. 54 (2019) 13740–13752, https://doi.org/10.1007/s10853-019-03882-1.
[43] M. Passi, B. Pal, A novel ternary Fe(III)-SrTiO3-GO nanocomposite for LED-light-driven photocatalytic degradation of norfloxacin antibiotic: performance, mineralization ability, degradation pathway, and mechanistic insight, Chem. Eng. J. 479 (2024) 147685, https://doi.org/10.1016/j.cej.2023.147685.
[44] X. Chen, R. Zhuan, J. Wang, Assessment of degradation characteristic and mineralization efficiency of norfloxacin by ionizing radiation combined with Fenton-like oxidation, J. Hazard Mater. 404 (2021) 124172, https://doi.org/10.1016/j.jhazmat.2020.124172.
[45] L. Chen, X. Zuo, S. Yang, T. Cai, D. Ding, Rational design and synthesis of hollow Co3O4@Fe2O3 core-shell nanostructure for the catalytic degradation of norfloxacin by coupling with peroxymonosulfate, Chem. Eng. J. 359 (2019) 373–384, https://doi.org/10.1016/j.cej.2018.11.120.
[46] F. Cao, J. Wang, Y. Wang, J. Zhou, S. Li, G. Qin, W. Fan, An: in situ Bi-decorated BiOBr photocatalyst for synchronously treating multiple antibiotics in water, Nanoscale Adv. 1 (2019) 1124–1129, https://doi.org/10.1039/c8na00197a.
[47] Y. Sun, W. Wu, H. Zhou, Lignosulfonate-controlled BiOBr/C hollow microsphere photocatalyst for efficient removal of tetracycline and Cr(VI) under visible light, Chem. Eng. J. 453 (2023), https://doi.org/10.1016/j.cej.2022.139819.